nature structural & molecular biology

Cycles in spatial and temporal chromosomal organization driven by the circadian clock

Lorena Aguilar-Arnal[1], Ofir Hakim[2,4,5], Vishal R Patel[3,5], Pierre Baldi[3], Gordon L Hager[2] & Paolo Sassone-Corsi[1]

Dynamic transitions in the epigenome have been associated with regulated patterns of nuclear organization. The accumulating evidence that chromatin remodeling is implicated in circadian function prompted us to explore whether the clock may control nuclear architecture. We applied the chromosome conformation capture on chip technology in mouse embryonic fibroblasts (MEFs) to demonstrate the presence of circadian long-range interactions using the clock-controlled *Dbp* gene as bait. The circadian genomic interactions with *Dbp* were highly specific and were absent in MEFs whose clock was disrupted by ablation of the *Bmal1* gene (also called *Arntl*). We establish that the *Dbp* circadian interactome contains a wide variety of genes and clock-related DNA elements. These findings reveal a previously unappreciated circadian and clock-dependent shaping of the nuclear landscape.

Circadian rhythms govern a large variety of physiological and metabolic functions[1–3]. The molecular mechanisms that underlie circadian rhythmicity are organized as an intricate and hierarchical network of transcriptional-translational loops[4,5]. This coordinated circadian machinery confers rhythmicity to a substantial portion of the transcriptome. Approximately 10% of genomic transcripts present circadian fluctuations of their abundance in many tissues or synchronized cells in culture[6]. A number of transcription factors have been implicated in the regulation of circadian gene expression. In mammals, the core circadian transcription factors include the transcriptional activators CLOCK and BMAL1, which heterodimerize and drive the transcription of *Per1–Per3*, *Cry1–Cry3*, *Rev-Erbα* (also called *Nr1d1*) and *Rev-Erbβ* (also known as *Nr1d2*) and *Rora*, *Rorb* or *Rorc*. PER and CRY protein complexes inhibit CLOCK-BMAL1–driven transcriptional activity, thereby giving rise to an autoregulatory transcriptional feedback loop. REV-ERB and ROR are nuclear receptors with opposed transcriptional activities, and they dictate the expression of circadian genes such as *Bmal1*. Indeed, the core clock exerts control over the circadian expression of other transcription factors such as *Dbp*, *Tef*, *Nfil3* (also called *E4bp4*), *Id2*, *Hlf* and *Pgc1α* (also called *Ppargc1a*), which in turn impose circadian rhythmicity on the expression of downstream genes.

Accumulating evidence has shown that chromatin remodeling events are involved in circadian regulation[7,8]. At the molecular level, CLOCK–BMAL1 and PER–CRY complexes have been shown to interact with several epigenetic modifiers, such as JARID1a (also called KDM5A), EZH2, MLL1 (also called KMT2A), WDR5 and CBP-p300, and some histone deacetylases, including the NAD^+ dependent enzyme SIRT1 (refs. 9–14). Both genetic and pharmacological approaches have shown that histone modifiers are implicated in circadian control, which indicates that their coordinated actions are necessary to fine tune a dynamic circadian epigenome. Genome-wide studies comprising mainly chromatin immunoprecipitation sequencing (ChIP-seq) analyses on livers harvested from mice in a circadian fashion have demonstrated that the histone modifications that are introduced by the circadian epigenetic modifiers are indeed rhythmic at many of the circadian gene promoters. These include rhythmic changes in acetylation at histone H3 Lys9 and Lys14 and methylation at histone H3 Lys4 and Lys27 (refs. 13,15,16), which parallels the rhythmic recruitment of polymerase II[13,17].

Although these studies provide convincing evidence on the role of chromatin remodeling in circadian function, they do not explore whether nuclear topological organization is influenced by the clock. As the functional compartmentalization of the nuclear interior is being unraveled[18–20], the spatial positioning of genes and regulatory elements is becoming increasingly recognized as an important epigenetic regulatory layer[21–24]. Hence, the three-dimensional folding of chromosomes inside the nucleus has been investigated extensively by fluorescence *in situ* hybridization (FISH) and chromosome conformation capture (3C) techniques[25]. The outcomes of these studies have revealed a nonrandom distribution of interphase chromosomes in chromosome territories and in topologically associating domains with common epigenetic marks[26–28]. The positioning configurations of chromosomes and genes diverge between cell types, and they can vary in response to physiological processes such as transcriptional reprogramming, development or disease[29]. In this respect, the circadian

[1]Department of Biological Chemistry, Center for Epigenetics and Metabolism, University of California Irvine, Irvine, California, USA. [2]Laboratory of Receptor Biology and Gene Expression, National Cancer Institute (NCI), National Institutes of Health (NIH), Bethesda, Maryland, USA. [3]Department of Computer Science, Institute for Genomics and Bioinformatics, University of California Irvine, Irvine, California, USA. [4]Present address: The Mina and Everard Goodman Faculty of Life Sciences, Bar-Ilan University, Ramat-Gan, Israel. [5]These authors contributed equally to this work. Correspondence should be addressed to P.S.-C. (psc@uci.edu) or P.B. (pfbaldi@ics.uci.edu).

Received 17 April; accepted 8 August; published online 22 September 2013; doi:10.1038/nsmb.2667

clock provides an ideal framework to study the interplay between genome organization and a physiologically dynamic program. Moreover, a potential regulatory role for the circadian clock in coordinating the higher-order structure of the chromatin has been lacking. In this study we investigated the contribution of the circadian clock to the fine tuning of temporal changes in genome organization. To this end, we explored the circadian genomic interactome of the clock-controlled gene *Dbp* in MEFs. We found that the genomic interactions at the *Dbp* locus change in a way that parallels the circadian cycle progression and the expression of the gene, thereby delineating a *Dbp* circadian interactome. Notably, the *Dbp* circadian interactome was dependent on intact clock machinery, as it was not present in *Bmal1*-deficient MEFs. We also found that the *Dbp* interactome enclosed other circadian genes and was enriched in functionally related genes.

RESULTS

Circadian long-range genomic interactions

We applied the 3C-derived technique chromosome conformation capture on chip (4C)[30,31] to detect preferential interactions of the *Dbp* gene with other loci in the genome during the circadian cycle. We selected the *Dbp* gene because of its robust circadian expression that is dictated by rhythmic CLOCK–BMAL1 binding to E-box DNA elements located on its promoter and coding sequences[32,33]. More precisely, we designed the bait for the 4C experiment in a region within intron 2 containing two E boxes (**Supplementary Fig. 1a**)[34]. We synchronized wild-type (WT) MEFs along the circadian cycle with dexamethasone (DEX). Cyclic expression of *Dbp* displayed a peak 22 h after synchronization (circadian time (CT) 22) and followed a very robust pattern of circadian expression[32,34] (**Fig. 1a**). This oscillation was abolished when the circadian core machinery was perturbed, as demonstrated in *Bmal1*$^{-/-}$ MEFs (**Fig. 1a** and **Supplementary Fig. 1b**). We sought to follow the *Dbp* circadian interactome at a high temporal resolution during the circadian cycle. We harvested cells every 4 h from CT22, which was the peak of *Dbp* expression, to CT34, which corresponded to the trough in gene expression. We also included a time point 12 h later, CT46, which corresponded to the peak of the second expression cycle (**Fig. 1a**, blue arrows). We performed 4C analyses on the *Dbp* genomic locus at the selected time points as described previously[31,35]. On average, about 75% of the positive probes (probe *p* score ($-\log_{10} P$ value) > 4; Online Methods) mapped to chromosome 7, which allocates the *Dbp* locus. This observation is consistent with the spatial organization of the genome into chromosome territories, which is a known feature of almost all eukaryotic cells[27,36,37]. On the basis of this notion, we adapted the 4C protocol to enhance the detection of interchromosomal (*trans*) contacts (ref. 35 and Online Methods).

To explore interaction frequencies in *trans*, we applied a running mean procedure to the mouse genome using a window size of 100 kb that was centered at each probe of the microarray. This analysis showed precise distribution and nonrandom interaction patterns for the *Dbp* locus that were coherent with the interaction patterns described previously for other loci in several cell types[35,38]. The genomic distribution of *Dbp* contacts along the circadian cycle remained largely unaltered and delineated the genomic spatial environment of the *Dbp* locus (**Fig. 1b–d** and **Supplementary Figs. 2** and **3**).

We identified 201 genomic regions that contact the *Dbp* gene at any time of the circadian cycle in WT MEFs, and the mean length of these regions was ~130 kb (**Fig. 1b** and **Supplementary Table 1**). Whereas some chromosomes, such as chromosomes 1, 3 and 12, interacted only rarely with *Dbp*, others displayed preferential contacts with our bait on different locations (**Fig. 1b**, outer layer). For example, on chromosome 11, we found 39 loci that contact *Dbp*. This result indicates close spatial proximity and a high intermingling frequency between territories from chromosomes 7 and 11 (refs. 39–41). Notably, the *Dbp* genomic contacts displayed a four-fold enrichment

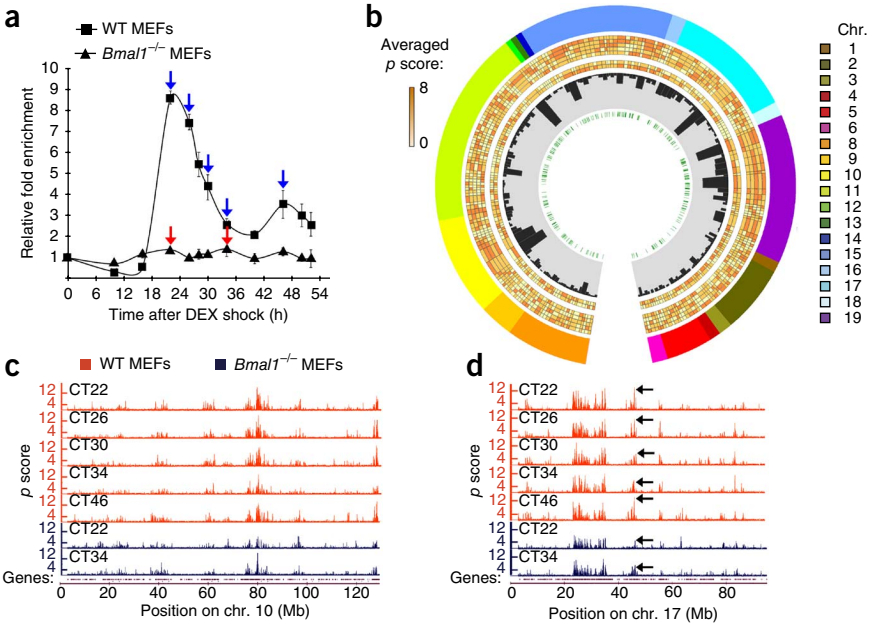

Figure 1 Characterization of genomic long-range interactions during the circadian cycle. (**a**) *Dbp* expression profile in WT and *Bmal1*$^{-/-}$ MEFs after synchronization with DEX, as analyzed by quantitative RT-PCR. The value at time 0 was set to 1. The data were normalized to *β-actin* (also known as *Actb*) and are represented as the average ± s.e.m. of three independent biological replicates. Blue and red arrows indicate the CT in which WT and *Bmal1*$^{-/-}$ cells, respectively, were harvested for 4C analysis. (**b**) Circos plot representing the *Dbp* interactome. The layers indicate, from the outside to the inside: chromosome, where the chromosome number is indicated as a color code and its length is proportional to the actual length of the interacting regions; averaged *p* scores for each genomic region shown as a color scale; histogram bars representing the gene content for each region; and E-box element locations. The averaged *p* scores correspond to each of the 4C experiments, from the outside to the inside: WT CT22, WT CT26, WT CT30, WT CT34, WT CT46, *Bmal1*$^{-/-}$ CT22 and *Bmal1*$^{-/-}$ CT34. (**c**,**d**) Microarray profiles showing the interaction frequencies (*p* scores from the 4C data) between *Dbp* and mouse chromosomes (chr.) 10 (**c**) and 17 (**d**). The orange and blue plots represent the data for WT and *Bmal1*$^{-/-}$ MEFs, respectively. The corresponding CT is indicated for each lane. The data sets are highly correlated, but major differences in the interaction frequencies are also apparent (black arrows in **d**). The genomic positions in mm8 coordinates are indicated on the horizontal axis. The profiles for the rest of the chromosomes are shown in **Supplementary Figure 3**.

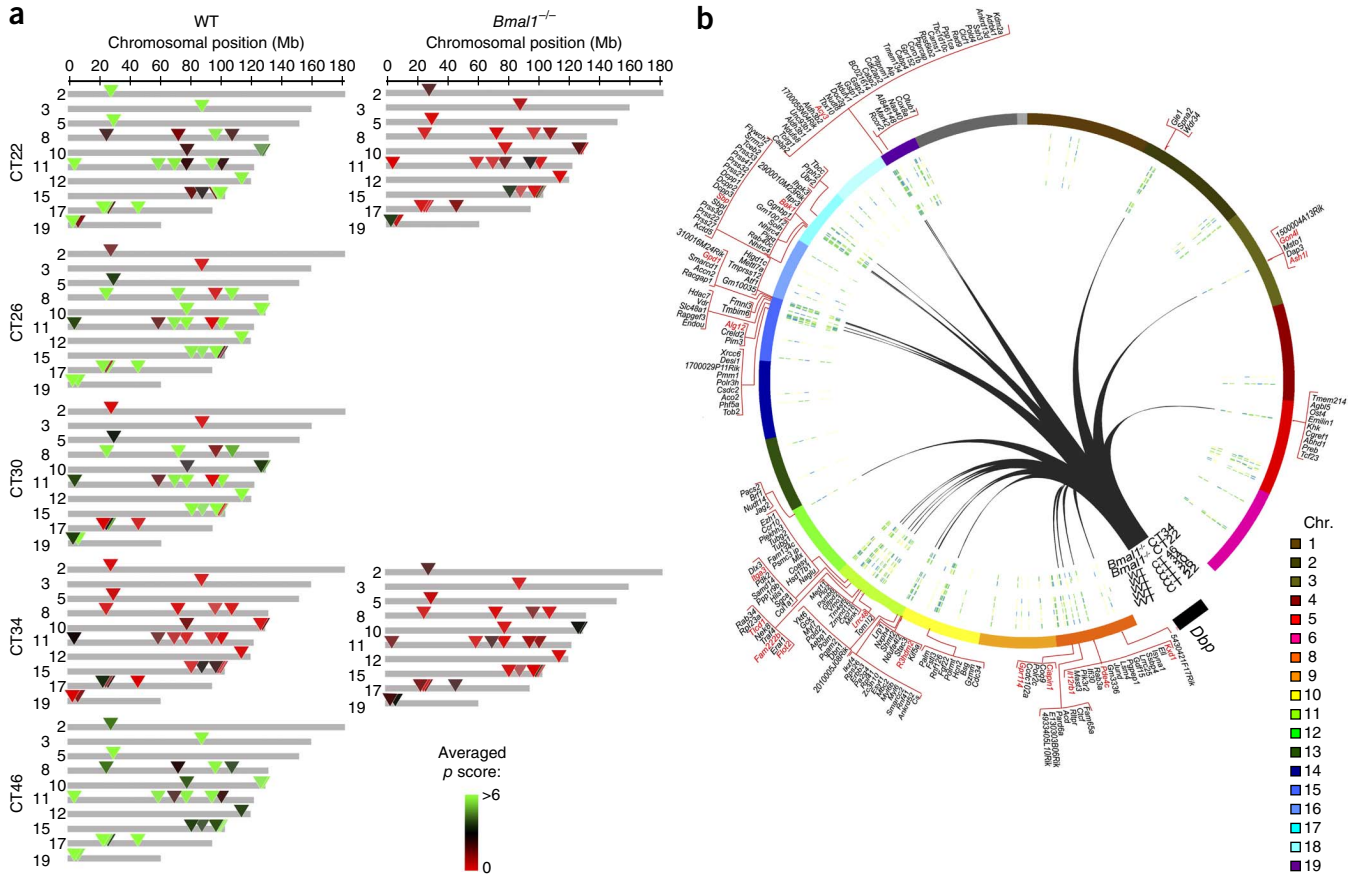

Figure 2 Genomic locations of *Dbp* long-range contacts that follow a BMAL1-dependent circadian pattern of interaction. (**a**) Genomic map of the *Dbp* circadian interactome at the indicated CTs after synchronization with DEX in WT and *Bmal1*$^{-/-}$ MEFs. Averaged *p* scores for each region are indicated in a green-red color scale according to the intensity of the interaction, which is proportional to the probe signal (4C over genomic DNA). Colored triangles indicate the positions of the *Dbp* circadian contacts. Areas shown in gray did not show circadian contact. The genomic positions in mm8 coordinates are indicated on the top horizontal axis. Chromosomes that did not present circadian interaction with *Dbp* are not shown here. (**b**) Circos plot representing the genome-wide view of *Dbp* circadian interactions (black lines) with the corresponding chromosomes *in trans*. The gene content corresponding to each contact region is indicated in the outer layer of the plot. The genes in red are those that presented circadian mRNA accumulation after synchronization with DEX as defined by the gene expression analysis (JTK $P < 0.01$).

in gene content over randomized data. This finding is consistent with previously described genomic contacts for active loci[31,35,38,42,43]. In agreement with previous studies, we found the highest running mean values in the 4C data for *Dbp* at chromosomal locations with high gene density[31,35,44] (**Supplementary Table 2** and **Supplementary Figs. 3** (with plots for chromosomes 10, 17, 18 and 19 shown as examples) and **4a**). This high enrichment for genes on specific regions interacting with *Dbp* (black histogram bars in the third layer in **Fig. 1b**) reflects the spatial distribution of chromatin domains, where active and gene-dense domains tend to colocalize[26,27,45]. We obtained similar results when we analyzed a parallel 4C experiment in which we synchronized a different MEF cell line and collected samples at CT22 and CT34 (**Supplementary Fig. 5**).

We then sought to determine the dynamics of the interaction of *Dbp* contacts during the circadian cycle. Our running mean analysis showed that the genomic locations of *Dbp* contacts remained similar overall along the circadian cycle. Notably, the interaction frequencies of *Dbp* with specific loci varied in degrees according to the locus and CT (**Fig. 1d**, with examples indicated by black arrows on the colored genomic plots).

To determine the overall likelihood of interaction of the *Dbp* locus with a given genomic region, we calculated an averaged *p* score for each of the 201 described contacts at each CT. We calculated the averaged *p* score by considering the *p* scores of neighboring probes (Online Methods). We then classified the *Dbp* genomic contacts according to their averaged *p* score at each CT. Interestingly, specific contacts that followed a cyclic pattern of interaction mirrored *Dbp* circadian gene expression. These genomic regions efficiently contact *Dbp* at CT22, CT26 and CT48, which corresponds to times at which *Dbp* shows the highest expression. These interactions were virtually undetectable at CT34, which is the time of lowest *Dbp* expression (**Fig. 2a**). We identified 29 genomic regions that met these criteria, and these regions comprise the *Dbp* circadian interactome (**Fig. 2b**, **Supplementary Fig. 4** and **Supplementary Table 3**).

Bmal1 is essential for a specific circadian interactome

We next sought to determine whether the molecular mechanism involved in establishing the *Dbp* circadian interactome implicates the clock machinery. To this end, we used *Bmal1*$^{-/-}$ MEFs (**Supplementary Fig. 1a**). BMAL1 is a basic helix-loop-helix transcription factor that heterodimerizes with another basic helix-loop-helix circadian transcription factor, CLOCK. These dimers bind in a precise time-of-day–dependent manner to E-box elements within circadian gene promoters to drive cyclic expression of genes[46,47].

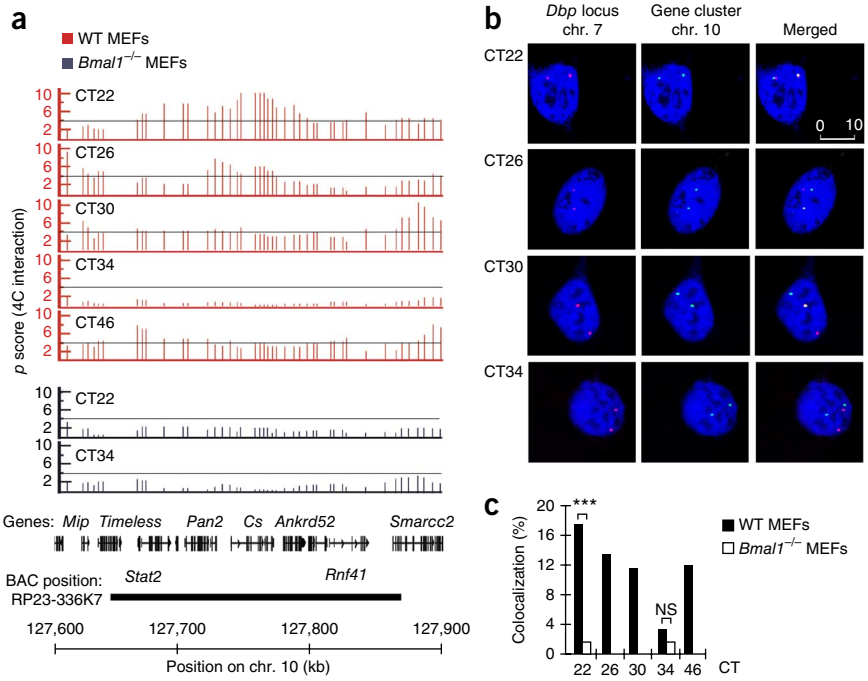

Figure 3 FISH validation of 4C data. (**a**) 4C microarray profiles for a selected region on chromosome 10 showing the running mean enrichments of the 4C signal over the genomic signal for 100-kb windows (*p* scores). The threshold for significance of the probes (*p* score = 4) is indicated by a gray line. The corresponding CT after synchronization with DEX is indicated on the top left for each plot. Orange plots represent data for WT MEFs, and the data corresponding to *Bmal1*$^{-/-}$ MEFs are shown in the blue plots. The gene positions and genomic locations in mm8 coordinates for all the plots are indicated at the bottom of the figure. The region covered by the bacterial artificial chromosome (BAC) used as a probe for this experiment is also indicated. (**b**) Representative double-labeled DNA-FISH for the *Dbp* locus on chromosome 7 (red) and the selected region on chromosome 10 (green). DNA was counterstained with DRAQ5 (blue). Representative picture shots correspond to WT MEFs synchronized with DEX and fixed for FISH analysis at the indicated CTs. $n = 288–342$ nuclei analyzed for each time point and genotype using three biological replicates. The scale bar in the top right image is in µm. (**c**) The interchromosomal interaction frequencies between *Dbp* and the selected gene cluster on chromosome 10. DEX-synchronized WT and *Bmal1*$^{-/-}$ MEFs were fixed at the indicated CTs for further DNA-FISH analysis. The data are shown as a percentage of colocalization on the basis of overlapping events of the green (chromosome 10 locus) and red (*Dbp* locus on chromosome 7) FISH probes from a total of 288–342 cell nuclei at each condition from three biological replicates (WT MEFs: CT22, $n = 315$; CT26, $n = 288$; CT30, $n = 307$; CT34, $n = 308$; CT46, $n = 342$. *Bmal1*$^{-/-}$ MEFs: CT22, $n = 322$; CT32, $n = 313$). $^{***}P = 4.18 \times 10^{-13}$. NS, nonsignificant ($P = 0.2$). Statistical significance was calculated by two-tailed Fisher's exact test.

Ablation of BMAL1 markedly disrupted circadian gene expression (**Fig. 1a**)[48]. We performed a 4C analysis using *Bmal1*$^{-/-}$ MEFs at CT22 and CT34 after stimulation with DEX. The time points CT22 and CT34 correspond to the peak and trough, respectively, of *Dbp* expression (**Fig. 1a**, red arrows). The *Dbp* contacts in the *Bmal1*$^{-/-}$ MEFs were similar overall to those in WT MEFs and showed a highly correlated profile of peaks and troughs (**Fig. 1c,d** and **Supplementary Figs. 2** and **3**). However, there was a markedly reduced contact frequency within the *Dbp* circadian interactome in *Bmal1*$^{-/-}$ MEFs (**Fig. 2a** and **Supplementary Table 3**). Notably, a lack of BMAL1 was associated with a loss of circadian oscillation in the interaction of *Dbp* with the 29 selected genomic regions (**Fig. 2a** and **Supplementary Table 3**). The profiles of the *Dbp* circadian contacts at both CT22 and CT34 in *Bmal1*$^{-/-}$ MEFs showed low interaction frequencies and were thus highly similar to the profile in WT MEFs at CT34 (**Fig. 2a**). These findings indicate that the circadian system contributes to the establishment of a specific subnuclear genomic environment around the *Dbp* gene.

To gain insights into the molecular mechanisms that contribute to the specific circadian genomic architecture of the *Dbp* locus, we used MotifMap[49] to identify the transcription-factor binding sites on the promoters of the genes that associate with *Dbp* in a circadian fashion (**Fig. 2b** and **Supplementary Table 4**). Among these promoters, we found a 2.5-fold enrichment on promoters containing E boxes ($P < 0.001$, Fisher exact test) (**Supplementary Table 4**). E boxes are highly conserved DNA elements that bind CLOCK-BMAL1 and are involved in driving circadian gene expression[32,50]. We speculate that the *Dbp* gene is present within a subnuclear environment that is gradually modified during the circadian cycle and that the circadian molecular machinery is implicated in establishing this pattern.

Visualizing *Dbp*-specific circadian interactions

To confirm the cyclic variations in the subnuclear localization of the *Dbp* locus that we observed by 4C, we performed DNA-FISH. As an example, we report the interchromosomal contact of *Dbp* with a high–gene content region on chromosome 10 that presents a very robust circadian profile of interaction that peaks at CT22 (**Fig. 3a** and **Supplementary Table 5**). The interaction frequency progressively decreased during the circadian cycle and was very low at CT34, but it increased again at CT46 (**Fig. 3a**). These cyclic interactions were abolished in *Bmal1*$^{-/-}$ MEFs, in which the frequency of interaction was low and was approximately equivalent at both CT22 and CT34 (**Fig. 3a** and **Supplementary Table 5**). We treated synchronized WT and *Bmal1*$^{-/-}$ MEFs for FISH analysis at various selected CTs (**Fig. 3b**). We analyzed DNA-FISH signals from 288–342 cells and monitored them for fluorescence colocalization of red and green signals, whose overlapping generates a visible yellow signal. We found a marked correlation between the interaction probability from the 4C signal and the colocalization frequency revealed by DNA-FISH (**Fig. 3**). There was a significant increase in the colocalization signals from the two loci at CT22 in WT MEFs compared to *Bmal1*$^{-/-}$ MEFs at the same CT (**Fig. 3c**; WT, 17.4%; *Bmal1*$^{-/-}$, 1.5%; $P < 0.001$, Fisher's exact test). WT MEFs showed a gradual decrease in colocalization events as the circadian cycle progressed. At CT34, a much smaller proportion of nuclei showed colocalization signals (WT, 3.2% of the MEFs; *Bmal1*$^{-/-}$, 1.4% of the MEFs; not significant ($P = 0.2$) by Fisher's exact test). We visualized the colocalization again 12 h later (**Fig. 3c**). The range of colocalization frequencies was optimal for interacting loci analyzed by FISH techniques[44]. The colocalization required a functional clock, as demonstrated by the analyses of *Bmal1*$^{-/-}$ MEFs. Thus, the circadian machinery contributes to the adequate *Dbp* genomic location in a precise subnuclear environment.

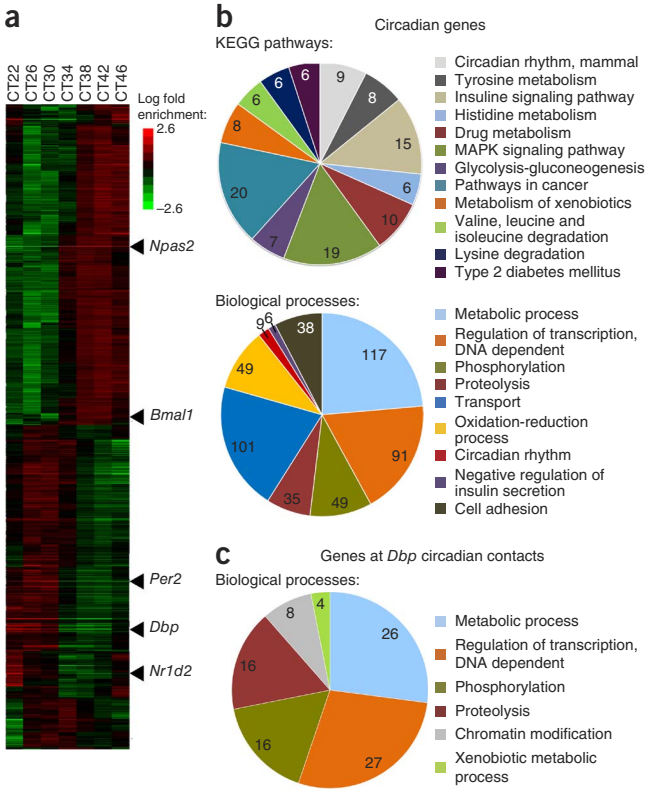

Figure 4 Circadian gene expression profiles in DEX-synchronized MEFs. (**a**) Heat map view of the global hierarchical cluster analysis of genes expressed in WT MEFs on a circadian basis. Each gene is represented as a horizontal line ordered vertically by phase as determined by Cluster 3.0. mRNA was extracted from WT MEFs every 4 h after synchronization with DEX, and microarray analyses were done in triplicate using the GeneChip Mouse Gene 1.0 ST Array. Some of the genes that comprise the circadian machinery are indicated as examples. (**b**,**c**) Pie charts representing the functional categories of circadian genes in WT MEFs (**b**) and the categories of genes that are present on the 4C genomic regions that interact with *Dbp* on a circadian basis (**c**). The numbers of genes sharing common biological processes are shown. The key shows the functional categories used to classify the genes. KEGG, Kyoto Encyclopedia for Genes and Genomes. The *P* values for each functional category are given in **Supplementary Table 7**.

Circadian contacts in a functionally specific network of genes

Higher-order genome organization has a major role in efficient responses to stimuli, effective signaling pathways and the coordination of lineage-specific differentiation[44,51,52]. Our observations prompted us to question whether the genes within the *Dbp* circadian interactome could be functionally related. There is a lack of comprehensive information on circadian gene expression profiles in MEFs. To overcome this hurdle, we performed a high-resolution circadian gene–expression microarray analysis on MEFs. We synchronized cells with DEX and collected total mRNA every 4 h during the 24-h circadian cycle starting at CT22. Out of ~28,000 transcripts analyzed in the microarrays, a total of 1,189 (~4%) displayed significantly rhythmic profiles (JTK $P < 0.01$, false discovery rate (FDR) < 5%; **Supplementary Table 6** and **Supplementary Fig. 4a**). We used hierarchical cluster analysis of the anchored data to order the genes by phase (**Fig. 4a**). The mRNAs from *Dbp* and other circadian components (*Per2*, *Per3*, *Bmal1*, *Npas2*, *Cry1*, *Cry2*, *Nr1d1* and *Nr1d2*) showed a very robust circadian oscillatory pattern (**Supplementary Fig. 6a**,**b**). These data confirmed that, as previously described, the transcriptional program in WT MEFs oscillates systematically and gradually during the circadian cycle.

The analysis of statistically enriched biological annotations in the identified circadian genes with respect to the mouse genome (**Fig. 4a** and **Supplementary Table 7**) revealed a significant enrichment of genes involved in metabolic processes ($P = 7.94 \times 10^{-14}$, hypergeometric test corrected by Benjamini and Hochberg post-test). These processes include lipid, carbohydrate and nucleotide metabolism. We identified many genes encoding transcriptional regulators. Among these genes, 8 participate in chromatin remodeling processes and 36 are known transcription factors. There was also a significant enrichment in proteins that are involved in oxidation-reduction processes ($P = 1.49 \times 10^{-9}$, hypergeometric test corrected by Benjamini and Hochberg post-test), most of which consist of proteins or enzymes that bind metabolites (NAD^+, NADH, FAD or heme) that regulate their catalytic activity. Several biological pathways were significantly enriched in our data set, including mammalian circadian rhythms ($P = 1.54 \times 10^{-6}$), amino acid metabolic pathways ($P = 1.29 \times 10^{-3}$) and insulin signaling and xenobiotic metabolism ($P = 1.14 \times 10^{-3}$; hypergeometric test corrected by Benjamini and Hochberg post-test) (**Fig. 4b** and **Supplementary Table 7**). Our findings are consistent with previous reports describing circadian genes and biological pathways[13,53–55].

These data prompted us to investigate whether common features are shared among the circadian transcriptome and the genetic content of the *Dbp* circadian contacts. There are 256 genes in the *Dbp* circadian interactome (**Fig. 2b**, outer layer, and **Supplementary Table 3**). We analyzed these genes to decipher their gene ontology enrichments (**Fig. 4c** and **Supplementary Table 7**). When we compared the biological functions in both groups of genes, we found a parallel between the genes expressed in a circadian manner in WT MEFs and those contained in the *Dbp* circadian interactome (**Fig. 4b**,**c** and **Supplementary Table 7**). The two most enriched ontological groups were those related to metabolic processes and the regulation of transcription (**Supplementary Table 7**). Both gene groups were enriched for the phosphorylation and proteolysis biological processes. Moreover, among the genes in *Dbp* circadian contacts, there was a significant enrichment for genes involved in xenobiotic metabolism ($P = 0.02$, hypergeometric test corrected by Benjamini and Hochberg post-test) (**Fig. 4c** and **Supplementary Table 7**), which is a process that is under circadian control[54,56]. DBP itself is a circadian-controlled transcription factor that confers rhythmicity to downstream target genes through binding to D-box consensus promoter sequences. Interestingly, DBP has been shown to specifically modulate xenobiotic metabolism[57]. In this context, the rhythmicity of the transcriptome and a time-controlled spatial nuclear organization could generate specialized environments that are involved in cyclic nuclear functions[35,44].

Features of genes within the *Dbp* circadian interactome

We next investigated the time-specific expression of genes within the *Dbp* circadian interactome. By comparing our circadian array data in MEFs with the genes that appear to have circadian contacts, we found 18 genes that cycle in a circadian manner (JTK $P < 0.01$) (**Figs. 2b**, genes in red, and **5a**, **Supplementary Fig. 4a** and **Supplementary Table 8**). These genes can be classified according to their expression phase into two major groups containing 5 and 13 genes (**Fig. 5a**). We confirmed the rhythmicity of the selected genes by RT-PCR and found that their mRNA levels oscillated in a circadian manner, further validating our microarray data (**Fig. 5b**).

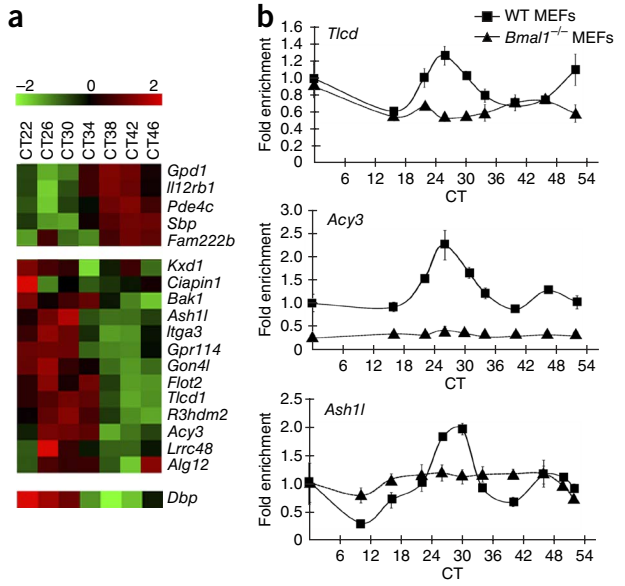

Figure 5 Circadian expression of *Dbp* and genes located in spatial proximity. (**a**) Heat map showing the $\log_2$ expression values of the circadian genes in the *Dbp* circadian interactome. Selected genes were plotted according to their phase. (**b**) Quantitative real-time PCR of selected transcripts confirming the microarray data. Total RNA was collected before synchronization with DEX (CT0) and at 16, 22, 26, 30, 34, 40, 46 and 52 h after DEX induction from WT and *Bmal1*$^{-/-}$ MEFs. Data were normalized to *β-actin* and are shown as the average ± s.e.m. of three independent biological replicates.

A motif discovery analysis on the promoters of these 18 genes revealed enrichment of recognition motifs for ROR-α and E-box elements (**Supplementary Fig. 6c**), which are known to be centrally implicated in circadian gene expression[58]. A comparative analysis with available BMAL1 ChIP-seq databases[13,47] indicated that the promoters of many genes located within the *Dbp* circadian interactome bind BMAL1 (**Supplementary Fig. 6d**). Moreover, the motif analysis indicated that the promoters of the circadian genes within the *Dbp* interactome may also contain D boxes (**Supplementary Fig. 6e**). These findings, which are consistent with our microarray analysis, suggest the possibility that the clock machinery itself could be implicated in shaping the nuclear genomic architecture.

DISCUSSION

The coordinated expression of circadian genes represents a remarkable paradigm of transcriptional control[6]. Accumulating evidence has recently shaped the notion that distinct changes in chromatin remodeling may be driven by the circadian clock to insure co-regulation of clock-controlled genes. The combined effects exerted by a variety of chromatin remodelers are assumed to lead to circadian activation and silencing of specific genes. Recent advances in the field of nuclear architecture have suggested that chromosome organization has an active role in many genomic functions. In this context, understanding how the nuclear landscape is modified in a CT-specific manner can lead to insights into the molecular mechanisms that determine circadian rhythms.

Our data reveal that the circadian clock is implicated in shaping temporal and spatial cycles in chromosomal organization. These variations in nuclear organization could provide a genomic frame to assist circadian gene expression of *Dbp*. Our data suggest that the genomic environment of the *Dbp* locus around the circadian cycle remains largely constant. However, several large chromatin domains change their frequency of interaction in *trans* with *Dbp*, which parallels the progression of the circadian cycle and the transcriptional state of the gene (**Fig. 2**). We present genetic evidence that BMAL1 has a critical role in establishing a CT-specific *Dbp* interactome (**Figs. 2** and **3**).

The outcomes of our comprehensive analysis have direct functional implications. In this respect, we described a spatial clustering of genes and circadian-related DNA elements around the *Dbp* locus. These results point to the existence of subnuclear environments enriched with CLOCK-specific response elements. This finding is in agreement with previous reports showing that spatial congregation of DNase I–hypersensitive sites is observed within DNA sequences that establish *trans* contacts[27,35]. The role of specific transcriptional regulators in establishing the interactome is emerging as a new avenue for understanding the modulation and functions of genome topology[59,60]. Here we provide evidence supporting the circadian clock, including the BMAL1 transcription factor, being involved in shaping the nuclear architecture during the circadian cycle. This conclusion is further reinforced by our study on BMAL1-deficient cells, in which the changes in the interactome around the circadian cycle were not present. Future studies will be necessary to uncover the precise contribution and the hierarchical organization of all clock regulators in determining circadian genome topology.

Notably, the analysis of the *Dbp* circadian interactome revealed a group of circadian genes whose transcript levels oscillate in a BMAL1-dependent fashion. Although the enrichment of functionally related genes in a time-specific manner favors a scenario in which particular genomic environments assist the coordinated transcription of a program of gene expression[19,60], additional experiments will be needed to support this point. Indeed, we cannot rule out the possibility that spatial clustering of functionally related genes appears to be a consequence of specific transcriptional regulators delineating the nuclear landscape during the circadian cycle. In this respect, it is possible that our study represents a paradigm for the function-structure-function model[29] in which genome activity drives genome topology, which in turn impinges on the functions of the genome. In this model, the stochastic nature of gene expression becomes modulated by the genomic environment[29] (**Fig. 6**). In this scenario, the circadian expression of

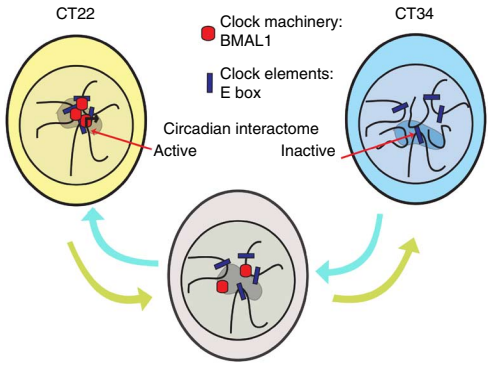

Figure 6 A schematic model of the cyclic events in chromosomal organization along the circadian cycle. Shown is a hypothetical model of cyclic long-range chromosomal interactions dictated by the circadian clock. During the CT that corresponds to high *Dbp* gene expression (CT22), a specific genomic environment is associated with gene transcription (represented by the shaded area in the nuclei of the cells). Genes participating in this process comprise the circadian interactome. As the circadian cycle progresses, the clock machinery is disassembled, and circadian gene expression decreases. When *Dbp* circadian transcription is at its trough (CT34), the clock machinery is already uncoupled from the E boxes, and this event correlates with a different genomic environment around the *Dbp* locus.

Dbp is dictated by the genomic environment to some extent (**Fig. 6**), and gene positioning could be a key modulatory factor. However, further experiments will be necessary to elucidate to what extent genome topology controls circadian gene expression and vice versa. The development of new technologies that allow the direct manipulation of specific genomic loci on a subnuclear scale will help provide more insights into this question. In addition, it could be hypothesized that the availability of specific metabolites or other events related to the cell cycle may also contribute to establishing the described circadian interactome. The cyclic changes that we observed here could also be implicated in other nuclear, nontranscriptional functions.

Although so far there has been a lack of solid biochemical approaches that allow for the deciphering of molecular mechanisms implicated in the organization of the circadian interactome, the conceptual advance derived from this research involves the notion that the circadian clock is able to operate on the physical organization of the nuclear landscape. Our data open new avenues for understanding the global coordination of circadian gene expression. We reason that circadian genome topology could be further studied in the context of circadian-related pathological conditions.

METHODS

Methods and any associated references are available in the online version of the paper.

Accession codes. All the microarray data have been deposited in the NCBI GEO database under the accession number GSE49639.

Note: Any Supplementary Information and Source Data files are available in the online version of the paper.

ACKNOWLEDGMENTS

We thank R.L. Schiltz and T.A. Johnson (NCI, NIH) for assisting with cell culture; R. Orozco-Solis, K. Eckel-Mahan, S. Sahar (Center for Epigenetics and Metabolism, University of California Irvine) and M. Groudine (Fred Hutchinson Cancer Research Center) for critical reading of the manuscript; S. Dilag (Center for Epigenetics and Metabolism, University of California Irvine) for technical support; X. Kong (Department of Biological Chemistry, University of California Irvine) for sharing FISH expertise and reagents; and all the members of the P.S.-C., G.L.H. and P.B. laboratories for discussions. This work was supported in part by the following grants: European Molecular Biology Organization (EMBO) long-term fellowship ALTF 411-2009 (to L.A.-A.), NIH grants R01-GM081634, AG041504 and AG033888 (to P.S.-C.) and Sirtris Pharmaceuticals grant SP-48984 (to P.S.-C.). The work of V.R.P. and P.B. is supported by the following grants: National Science Foundation grant IIS-0513376 and NIH grants LM010235-01A1 and 5T15LM007743 (to P.B.).

AUTHOR CONTRIBUTIONS

L.A.-A., O.H., G.L.H. and P.S.-C. conceived and designed the research. L.A.-A. and O.H. performed 4C experiments. L.A.-A. performed FISH and gene expression experimental work. L.A.-A., O.H., V.R.P. and P.B. performed bioinformatical analyses. V.R.P. performed promoter analyses using MotifMap. L.A.-A. and O.H. analyzed and interpreted the data. L.A.-A. and P.S.-C. wrote the manuscript.

COMPETING FINANCIAL INTERESTS

The authors declare no competing financial interests.

1. Bass, J. Circadian topology of metabolism. *Nature* **491**, 348–356 (2012).
2. Schibler, U. & Sassone-Corsi, P. A web of circadian pacemakers. *Cell* **111**, 919–922 (2002).
3. Wijnen, H. & Young, M.W. Interplay of circadian clocks and metabolic rhythms. *Annu. Rev. Genet.* **40**, 409–448 (2006).
4. Mohawk, J.A., Green, C.B. & Takahashi, J.S. Central and peripheral circadian clocks in mammals. *Annu. Rev. Neurosci.* **35**, 445–462 (2012).
5. Reppert, S.M. & Weaver, D.R. Coordination of circadian timing in mammals. *Nature* **418**, 935–941 (2002).
6. Doherty, C.J. & Kay, S.A. Circadian control of global gene expression patterns. *Annu. Rev. Genet.* **44**, 419–444 (2010).
7. Aguilar-Arnal, L. & Sassone-Corsi, P. The circadian epigenome: how metabolism talks to chromatin remodeling. *Curr. Opin. Cell Biol.* **25**, 170–176 (2013).
8. Feng, D. & Lazar, M.A. Clocks, metabolism, and the epigenome. *Mol. Cell* **47**, 158–167 (2012).
9. Asher, G. *et al.* SIRT1 regulates circadian clock gene expression through PER2 deacetylation. *Cell* **134**, 317–328 (2008).
10. DiTacchio, L. *et al.* Histone lysine demethylase JARID1a activates CLOCK-BMAL1 and influences the circadian clock. *Science* **333**, 1881–1885 (2011).
11. Etchegaray, J.P. *et al.* The polycomb group protein EZH2 is required for mammalian circadian clock function. *J. Biol. Chem.* **281**, 21209–21215 (2006).
12. Katada, S. & Sassone-Corsi, P. The histone methyltransferase MLL1 permits the oscillation of circadian gene expression. *Nat. Struct. Mol. Biol.* **17**, 1414–1421 (2010).
13. Koike, N. *et al.* Transcriptional architecture and chromatin landscape of the core circadian clock in mammals. *Science* **338**, 349–354 (2012).
14. Nakahata, Y. *et al.* The NAD^+-dependent deacetylase SIRT1 modulates CLOCK-mediated chromatin remodeling and circadian control. *Cell* **134**, 329–340 (2008).
15. Etchegaray, J.P., Lee, C., Wade, P.A. & Reppert, S.M. Rhythmic histone acetylation underlies transcription in the mammalian circadian clock. *Nature* **421**, 177–182 (2003).
16. Vollmers, C. *et al.* Circadian oscillations of protein-coding and regulatory RNAs in a highly dynamic mammalian liver epigenome. *Cell Metab.* **16**, 833–845 (2012).
17. Le Martelot, G. *et al.* Genome-wide RNA polymerase II profiles and RNA accumulation reveal kinetics of transcription and associated epigenetic changes during diurnal cycles. *PLoS Biol.* **10**, e1001442 (2012).
18. Hakim, O., Sung, M.H. & Hager, G.L. 3D shortcuts to gene regulation. *Curr. Opin. Cell Biol.* **22**, 305–313 (2010).
19. Rajapakse, I. & Groudine, M. On emerging nuclear order. *J. Cell Biol.* **192**, 711–721 (2011).
20. Sanyal, A., Lajoie, B.R., Jain, G. & Dekker, J. The long-range interaction landscape of gene promoters. *Nature* **489**, 109–113 (2012).
21. Giles, K.E., Gowher, H., Ghirlando, R., Jin, C. & Felsenfeld, G. Chromatin boundaries, insulators, and long-range interactions in the nucleus. *Cold Spring Harb. Symp. Quant. Biol.* **75**, 79–85 (2010).
22. Edelman, L.B. & Fraser, P. Transcription factories: genetic programming in three dimensions. *Curr. Opin. Genet. Dev.* **22**, 110–114 (2012).
23. Sexton, T., Bantignies, F. & Cavalli, G. Genomic interactions: chromatin loops and gene meeting points in transcriptional regulation. *Semin. Cell Dev. Biol.* **20**, 849–855 (2009).
24. Lanctôt, C., Cheutin, T., Cremer, M., Cavalli, G. & Cremer, T. Dynamic genome architecture in the nuclear space: regulation of gene expression in three dimensions. *Nat. Rev. Genet.* **8**, 104–115 (2007).
25. Bickmore, W.A. & van Steensel, B. Genome architecture: domain organization of interphase chromosomes. *Cell* **152**, 1270–1284 (2013).
26. Dixon, J.R. *et al.* Topological domains in mammalian genomes identified by analysis of chromatin interactions. *Nature* **485**, 376–380 (2012).
27. Lieberman-Aiden, E. *et al.* Comprehensive mapping of long-range interactions reveals folding principles of the human genome. *Science* **326**, 289–293 (2009).
28. Nora, E.P. *et al.* Spatial partitioning of the regulatory landscape of the X-inactivation centre. *Nature* **485**, 381–385 (2012).
29. Cavalli, G. & Misteli, T. Functional implications of genome topology. *Nat. Struct. Mol. Biol.* **20**, 290–299 (2013).
30. Ohlsson, R. & Gondor, A. The 4C technique: the 'Rosetta stone' for genome biology in 3D? *Curr. Opin. Cell Biol.* **19**, 321–325 (2007).
31. Simonis, M. *et al.* Nuclear organization of active and inactive chromatin domains uncovered by chromosome conformation capture-on-chip (4C). *Nat. Genet.* **38**, 1348–1354 (2006).
32. Ripperger, J.A. & Schibler, U. Rhythmic CLOCK-BMAL1 binding to multiple E-box motifs drives circadian Dbp transcription and chromatin transitions. *Nat. Genet.* **38**, 369–374 (2006).
33. Stratmann, M., Suter, D.M., Molina, N., Naef, F. & Schibler, U. Circadian Dbp transcription relies on highly dynamic BMAL1-CLOCK interaction with E boxes and requires the proteasome. *Mol. Cell* **48**, 277–287 (2012).
34. Wuarin, J. & Schibler, U. Expression of the liver-enriched transcriptional activator protein DBP follows a stringent circadian rhythm. *Cell* **63**, 1257–1266 (1990).
35. Hakim, O. *et al.* Diverse gene reprogramming events occur in the same spatial clusters of distal regulatory elements. *Genome Res.* **21**, 697–706 (2011).
36. Cremer, T. & Cremer, M. Chromosome territories. *Cold Spring Harb. Perspect. Biol.* **2**, a003889 (2010).
37. Zhang, Y. *et al.* Spatial organization of the mouse genome and its role in recurrent chromosomal translocations. *Cell* **148**, 908–921 (2012).
38. Hakim, O. *et al.* DNA damage defines sites of recurrent chromosomal translocations in B lymphocytes. *Nature* **484**, 69–74 (2012).
39. Ling, J.Q. *et al.* CTCF mediates interchromosomal colocalization between Igf2/H19 and Wsb1/Nf1. *Science* **312**, 269–272 (2006).
40. Mahy, N.L., Perry, P.E. & Bickmore, W.A. Gene density and transcription influence the localization of chromatin outside of chromosome territories detectable by FISH. *J. Cell Biol.* **159**, 753–763 (2002).

41. Zhao, Z. *et al.* Circular chromosome conformation capture (4C) uncovers extensive networks of epigenetically regulated intra- and interchromosomal interactions. *Nat. Genet.* **38**, 1341–1347 (2006).
42. Bian, Q. & Belmont, A.S. Revisiting higher-order and large-scale chromatin organization. *Curr. Opin. Cell Biol.* **24**, 359–366 (2012).
43. Shopland, L.S. *et al.* Folding and organization of a contiguous chromosome region according to the gene distribution pattern in primary genomic sequence. *J. Cell Biol.* **174**, 27–38 (2006).
44. Schoenfelder, S. *et al.* Preferential associations between co-regulated genes reveal a transcriptional interactome in erythroid cells. *Nat. Genet.* **42**, 53–61 (2010).
45. Gilbert, N. *et al.* Chromatin architecture of the human genome: gene-rich domains are enriched in open chromatin fibers. *Cell* **118**, 555–566 (2004).
46. Hogenesch, J.B., Gu, Y.Z., Jain, S. & Bradfield, C.A. The basic-helix-loop-helix-PAS orphan MOP3 forms transcriptionally active complexes with circadian and hypoxia factors. *Proc. Natl. Acad. Sci. USA* **95**, 5474–5479 (1998).
47. Rey, G. *et al.* Genome-wide and phase-specific DNA-binding rhythms of BMAL1 control circadian output functions in mouse liver. *PLoS Biol.* **9**, e1000595 (2011).
48. Bunger, M.K. *et al.* Mop3 is an essential component of the master circadian pacemaker in mammals. *Cell* **103**, 1009–1017 (2000).
49. Daily, K., Patel, V.R., Rigor, P., Xie, X. & Baldi, P. MotifMap: integrative genome-wide maps of regulatory motif sites for model species. *BMC Bioinformatics* **12**, 495 (2011).
50. Hardin, P.E. Transcription regulation within the circadian clock: the E-box and beyond. *J. Biol. Rhythms* **19**, 348–360 (2004).
51. Hadjur, S. *et al.* Cohesins form chromosomal *cis*-interactions at the developmentally regulated IFNG locus. *Nature* **460**, 410–413 (2009).
52. Kosak, S.T. *et al.* Coordinate gene regulation during hematopoiesis is related to genomic organization. *PLoS Biol.* **5**, e309 (2007).
53. Cho, H. *et al.* Regulation of circadian behaviour and metabolism by REV-ERB-α and REV-ERB-β. *Nature* **485**, 123–127 (2012).
54. Eckel-Mahan, K.L. *et al.* Coordination of the transcriptome and metabolome by the circadian clock. *Proc. Natl. Acad. Sci. USA* **109**, 5541–5546 (2012).
55. Panda, S. *et al.* Coordinated transcription of key pathways in the mouse by the circadian clock. *Cell* **109**, 307–320 (2002).
56. Claudel, T., Cretenet, G., Saumet, A. & Gachon, F. Crosstalk between xenobiotics metabolism and circadian clock. *FEBS Lett.* **581**, 3626–3633 (2007).
57. Gachon, F., Olela, F.F., Schaad, O., Descombes, P. & Schibler, U. The circadian PAR-domain basic leucine zipper transcription factors DBP, TEF, and HLF modulate basal and inducible xenobiotic detoxification. *Cell Metab.* **4**, 25–36 (2006).
58. Ueda, H.R. *et al.* System-level identification of transcriptional circuits underlying mammalian circadian clocks. *Nat. Genet.* **37**, 187–192 (2005).
59. Hakim, O. *et al.* Spatial congregation of STAT binding directs selective nuclear architecture during T cell functional differentiation. *Genome Res.* **23**, 462–472 (2013).
60. Schoenfelder, S., Clay, I. & Fraser, P. The transcriptional interactome: gene expression in 3D. *Curr. Opin. Genet. Dev.* **20**, 127–133 (2010).

ONLINE METHODS

MEF cultures. MEF cells were established from either WT mice or *Bmal1*-null mutant littermates[48], as is routinely done in our laboratory[61,62]. MEFs were maintained in DMEM supplemented with heat-inactivated 10% FBS (GibcoBRL), nonessential amino acids (Gibco) and antibiotics. Cells were cultured at 37 °C in 5% CO_2. The absence of BMAL1 protein was confirmed by western blotting using antibodies to BMAL1 (Abcam, Ab3350) at 1:2,500 dilution in Tris-buffered saline plus Tween-20 (TBST) and 5% nonfat milk. Antibodies to actin antibody (Abcam, Ab3280) at 1:10,000 dilution in PBST were used as a loading control.

RNA extraction and GeneChip analyses. RNA isolation for microarray analyses was done as previously described[12,63]. MEFs from WT mice were plated on six-well dishes and grown until confluence. For synchronization, cells were treated with 100 nM DEX in DMEM for 1 h[64]. The hormone was washed out twice with PBS, and supplemented DMEM was added to the cells. MEFs were harvested for RNA isolation at the CTs of interest, with the time of treatment being defined as CT0. For each time point, we prepared samples for the assay in triplicate. Total RNA was extracted using TRIzol reagent (Invitrogen) following the manufacturer's instructions. RNA was further cleaned using an RNeasy Mini Kit (Qiagen). RNA quality control was assayed using an Agilent 2100 Bioanalyzer platform, and RNA was quantified with a NanoDrop spectrophotometer. Probe synthesis and chip hybridization were performed at the University of California Irvine DNA Microarray Core Facility. Briefly, 100 ng of total RNA per sample was used as a template to obtain cDNA with the GeneChip cDNA synthesis Kit (Affymetrix). Mouse Gene 1.0 ST arrays (Affymetrix) were used to characterize gene expression levels during the circadian cycle in WT MEFs. Data were normalized, and for each probe set, the measurements of the three microarrays were averaged. For analysis of rhythmic transcripts, the nonparametric test JTK-cycle was used incorporating a window of 20–28 h for the determination of circadian periodicity[65]. The algorithm used by the JTK-cycle analysis is a combination of the Jonckheere-Terpstra test for monotonic ordering and Kendall's τ test for association of measured quantities. It is optimized for the detection of rhythmicity. Transcripts were considered circadian if JTK $P < 0.01$. For this significance, an FDR was calculated by permutations of the data and corresponded to 5%. Circadian genes were clustered and heat maps were visualized using the software Cluster 3.0, Java Treeview[66,67] and MultiExperiment Viewer[68,69]. Briefly, $\log_2$-transformed expression values at the CTs analyzed for the selected circadian genes were centered at their mean so that the mean value for each gene was set to 0. Hierarchical clustering was then performed and visualized as a heat map.

Ontological analyses. Automated extraction of concurrent gene ontology annotations was performed with the GeneCodis program[70,71]. The gene ontology category 'biological processes' was selected and was extracted from http://www.geneontology.com. Biological pathways were extracted from http://www.genome.jp/kegg/ as 'KEGG pathways'. The *P*-value calculations with GeneCodis were performed using the hypergeometric-distribution statistical test[70,71]. The *P* values were then corrected by an implementation of the FDR method of Benjamini and Hochberg as described[70,71].

Quantitative real-time RT-PCR. cDNA was obtained by retrotranscription of 1 µg of total mRNA using the iScript cDNA synthesis kit (Bio-Rad) following the manufacturer's instructions. Real-time RT-PCR was done using the Chromo4 real-time detection system (Bio-Rad). The PCR primers for *Dbp* mRNA were described elsewhere[14]. For a 20 µl PCR, 50 ng of cDNA template was mixed with the primers to a final concentration of 200 nM and mixed with 10 µl of iQ SYBR Green Supermix (Bio-Rad). The reactions were done in triplicates using the following conditions: 3 min at 95 °C followed by 40 cycles of 30 s at 95 °C and 1 min at 60 °C.

4C. 4C assays were performed as described previously[31,35] with some modifications. For each experiment, 20 million cells were synchronized with DEX. Cross-linking was done in a final concentration of 2% formaldehyde at 37 °C for 10 min. The reaction was quenched by the addition of glycine (final concentration of 0.125 M). Cells were washed with cold PBS and lysed for 1 h at 4 °C with nuclear extraction buffer (10 mM Tris-HCl, pH 8.0, 10 mM NaCl, 0.2% NP-40 and 1× complete protease inhibitors (Roche)). Cells were collected by centrifugation, resuspended in 1 ml of restriction buffer (New England BioLabs Buffer 2) and kept frozen at −80 °C until all samples were harvested and processed. Once all the samples were ready, a final concentration of 0.3% SDS was added to 10 million cells and incubated at 37 °C for 1 h. Triton X-100 was then added to a final concentration of 1.8%, and samples were incubated for 1 h at 37 °C. Cross-linked DNA was digested with 500 U of HindIII (New England BioLabs) at 37 °C overnight. The enzyme was heat inactivated (65 °C for 30 min), and the reaction was resuspended in a total volume of 7 ml with 1× ligation buffer (Roche) and 100 U of T4 DNA Ligase (Roche) followed by incubation at 16 °C overnight. Samples were treated with 500 µg of Proteinase K (Ambion), and cross-linking was reversed at 65 °C overnight. DNA was phenol extracted and ethanol precipitated. 50 µg of this 3C template was digested overnight with 50 U of Csp6I enzyme (Fermentas). The enzyme was heat inactivated, and the DNA was phenol extracted, ethanol precipitated and subsequently ligated at a low concentration to promote circularization (that is, intramolecular ligation events) in a final volume of 7 ml with 100 U of T4 DNA Ligase (Roche). Ligation products were phenol extracted and ethanol precipitated using glycogen as a carrier.

PCR reactions were performed using the Expand Long Template PCR system (Roche). We used the maximum amount of template that still shows a linear amplification by testing serial dilutions of each sample and quantifying the PCR products in agarose gels using QuantityOne software. PCRs were done in a PTC-100 thermal cycler (Bio-Rad) using the following conditions: 2 min at 95 °C followed by 30 cycles of 15 s at 94 °C, 1 min at 60 °C and 3 min at 68 °C, and a final extension step of 7 min at 68 °C was included. *Dbp* bait was amplified with the following inverse primers: Dbp4CHindIII: 5′-TCACAGGGTTTATGCCTGACAGGAT-3′; Dbp4CCsp6I: 5′-AGCACTGGTTTTTGCCTGGCGGTC-3′. The position of the bait in *Dbp* locus and the restriction fragments are given in **Supplementary Figure 1a**. 16 PCR reactions were pooled and purified using the QIAquick nucleotide removal kit (Qiagen). 4C template DNA was hybridized to custom-made microarrays designed as described previously[35] using the mm8 assembly of the mouse genome. The hybridization of DNA samples for ChIP-chip analysis was performed by following the manufacturer's instructions with modifications. Briefly, 20 µg of the Cy5-labeled 4C sample and 20 µg of the Cy3-labeled reference sample (genomic DNA) were mixed, dried down and resuspended in 20 µl of NimbleGen Hybridization Buffer (NimbleGen Systems). After denaturation, hybridization was carried out in a MAUI Hybridization System (BioMicro Systems) for 24 h at 42 °C. The arrays were washed using the NimbleGen Wash Buffer System (NimbleGen Systems), dried by centrifugation and scanned in a two-color scanning system. Images were processed using ImageJ and Nimblescan software as reported in the user's guides.

The sequences located on chromosome 7 contacted the *Dbp* locus very frequently, and they were highly represented in the 4C DNA library. Subsequently, under these conditions, the labeling and hybridization process saturated the probes from chromosome 7 in the microarray, thereby generating nonquantitative data.

4C data analyses for quantitative interactions. Statistical analyses of the 4C microarray data were performed using the R environment implemented with the ACME package (http://www.bioconductor.org/packages/release/bioc/html/ACME.html), as reported previously[35]. Briefly, the ratio of sample DNA to genomic DNA was calculated for each probe. Normalized data for each probe were $\log_2$ transformed. Using a procedure consisting of a running-window χ^2 test of 100-kb windows centered at the probe, a *P* value was generated for each probe. The data was $\log_{10}$ transformed, and thus a $-\log_{10} P$ value was assigned to each probe as a measure of its interacting frequency. The $-\log_{10} P$ value is called the *p* score in the main text and figures. Probes with a $-\log_{10} P$ value or *p* score greater than 4 in at least one of the time points were selected as being positive, which corresponded to an FDR of ~0.3%.

The 100-kb flanking regions around the probes having *p* scores within the top 0.1% were extracted and were considered significant. Overlapping regions were further merged to get a set of 201 nonoverlapping regions with a mean length of 130 kb. When several regions are merged, their $-\log_{10} P$ values or *p* scores are averaged in a procedure that generates the averaged *p* score. This procedure was carried out at different window lengths and *p*-value cutoffs, but there was no qualitative change in the results. The procedure produced 201 nonoverlapping regions with a time-series profile of their interactions with the *Dbp* bait as measured by their $-\log_{10} P$ value at each time point. Using *K*-means clustering with Pearson correlation as the similarity metric, the interaction profiles were

doi:10.1038/nsmb.2667

further clustered into 12 groups[72]. We selected the genomic regions of two of the clusters, which presented a difference of (averaged $-\log_{10} P$ value at CT22 or CT26) − (averaged $-\log_{10} P$ value at CT34) > 4. The selected regions were visually inspected in the *K*-means plots, which confirmed their cyclic pattern over the time points investigated. The genomic locations were viewed with the Integrated Genome Browser software (http://bioviz.org/igb/). FDR values were determined as previously described[35]. Briefly, permutations of the data generated randomized 4C values for all the genomic positions that were represented as probes in the microarray. A χ^2 test was performed on these data as described, which determined the FDR calculation by dividing the number of positive probes by the actual number of positive probes from the 4C microarray. All the genome analyses were converted to mm9 genomic coordinates and illustrated in **Supplementary Tables 1–3**.

DNA FISH. For three-dimensional FISH, MEFs were grown on UV-sterilized 22 × 22 mm coverslips placed onto six-well plates. Cells were synchronized with DEX and grown until the desired time point. Fixation was performed in 4% paraformaldehyde for 10 min. Cells were permeabilized in 0.5% saponin (Sigma), 0.5% Triton X-100 and 1× PBS for 20 min at room temperature. After two washes with 2× saline–sodium citrate (SSC) buffer, pH 7, cells were stored in 50% formamide and 2× SSC buffer, pH 7, for 2 h. We used BACs as templates for the probes, which we obtained from the BACPAC resources center. The identification numbers of the BACs used are as follows: RP23-36B116 for *Dbp* and RP23-100C9 and RP23-336K7 for the region in chromosome 10. BAC DNA was isolated and verified by PCR. 1 µg of BAC DNA was labeled by nick translation with either biotin (Roche, Biotin-Nick Translation Mix) or digoxigenin (DIG) (Roche, DIG-Nick Translation Mix) following the manufacturer's instructions. For each slide, 600 ng of probe was ethanol precipitated in the presence of 8 µg of mouse COT1 DNA (Invitrogen) and 40 µg of tRNA. The pellet was resuspended in 5 µl of formamide, and 5 µl of 2× hybridization buffer (20% dextran sulfate, 4× SSC and 2% Tween-20) was added. The probe was denatured together with the nuclei for 30 min at 80 °C and left to hybridize during two overnight periods at 37 °C in a humidified chamber. The nonhybridized probe was washed out with successive washes consisting of three washes with 50% formamide and 2× SSC for 5 min at 45 °C, three washes with 1× SSC for 5 min at 60 °C and one wash with 0.05% Tween-20 and 4× SSC at room temperature for 5 min. A blocking step was included with blocking solution (3% BSA, 0.05% Tween-20 and 4× SSC) for 30 min. Labeled probes were detected with a 1:200 dilution of fluorescein-avidin (Vector labs, A–3101) and rhodamine anti-DIG (Roche, 1207750) in blocking solution for 1 h at 37 °C in a humid chamber. The excess of fluorescent reagents was washed out by three 5-min washes at 45 °C with 0.05% Tween-20 and 4× SSC. DNA was counterstained with DRAQ5 (Biostatus) according to the manufacturer's protocol. Slides were mounted in Vectashield HardSet (Vector labs) and stored at 4 °C until visualization.

Microscopy and image analyses. We examined DNA-FISH signals on a Leica TSC SP5 confocal microscope with a 60× 1.4 immersion oil objective lens controlled by a Leica LAS System. We collected confocal stacks at randomly chosen fields and included all cells with clear signals for the four alleles in the analysis. We captured confocal stacks for these cells using green and red channels to detect both *Dbp* and the genomic locus on chromosome 10. A minimum of 250 cells were analyzed and scored for colocalization events by a person blind to the experimental sampling.

Promoter analyses. Genes overlapping 4C regions were identified using all known RefSeq[73] transcripts for the mouse genome. All gene promoters that overlapped regions from the 4C data were further analyzed for transcription-factor binding sites using the MotifMap database[49,74]. Briefly, in MotifMap, the mouse genome is searched for binding sites using position-specific weight matrices from TRANSFAC[75] and JASPAR[76]. The sites are then filtered with a combination of the motif-matching score (*Z*-score) and the conservation score (Bayesian branch length score (BBLS)). For this study, only sites with BBLS values greater than 1 were retained. Using all promoters (defined as 8 kb upstream and 3 kb downstream of the transcription start sites) in the mouse genome as a control (mm9), a Fisher test was performed to find transcription-factor binding sites that are specifically enriched in the promoters that overlap the 4C regions.

Motif discovery analysis was performed using the algorithm MEME 4.9.0, which is available at http://meme.nbcr.net/meme/cgi-bin/meme.cgi. The selected promoters were used as inputs in FASTA format, and output files were examined to retrieve matching motifs for known transcription factors. To perform this analysis, the discovered motifs were queried against the database JASPAR[76] using Tomtom.

Circos plots. Circos plots were constructed using the Circos software[77]. Data from the 4C experiment, the gene-overlap analysis and the transcription-factor binding-site analysis were used as input.

61. Hirayama, J. *et al.* CLOCK-mediated acetylation of BMAL1 controls circadian function. *Nature* **450**, 1086–1090 (2007).
62. Pando, M.P., Morse, D., Cermakian, N. & Sassone-Corsi, P. Phenotypic rescue of a peripheral clock genetic defect via SCN hierarchical dominance. *Cell* **110**, 107–117 (2002).
63. Grimaldi, B. *et al.* PER2 controls lipid metabolism by direct regulation of PPARγ. *Cell Metab.* **12**, 509–520 (2010).
64. Balsalobre, A. *et al.* Resetting of circadian time in peripheral tissues by glucocorticoid signaling. *Science* **289**, 2344–2347 (2000).
65. Hughes, M.E., Hogenesch, J.B. & Kornacker, K. JTK_CYCLE: an efficient nonparametric algorithm for detecting rhythmic components in genome-scale data sets. *J. Biol. Rhythms* **25**, 372–380 (2010).
66. Eisen, M.B., Spellman, P.T., Brown, P.O. & Botstein, D. Cluster analysis and display of genome-wide expression patterns. *Proc. Natl. Acad. Sci. USA* **95**, 14863–14868 (1998).
67. de Hoon, M.J., Imoto, S., Nolan, J. & Miyano, S. Open source clustering software. *Bioinformatics* **20**, 1453–1454 (2004).
68. Saeed, A.I. *et al.* TM4 microarray software suite. *Methods Enzymol.* **411**, 134–193 (2006).
69. Saeed, A.I. *et al.* TM4: a free, open-source system for microarray data management and analysis. *Biotechniques* **34**, 374–378 (2003).
70. Nogales-Cadenas, R. *et al.* GeneCodis: interpreting gene lists through enrichment analysis and integration of diverse biological information. *Nucleic Acids Res.* **37**, W317–W322 (2009).
71. Carmona-Saez, P., Chagoyen, M., Tirado, F., Carazo, J.M. & Pascual-Montano, A. GENECODIS: a web-based tool for finding significant concurrent annotations in gene lists. *Genome Biol.* **8**, R3 (2007).
72. Baldi, P. & Brunak, S. *Bioinformatics: The Machine Learning Approach.* 476 (MIT Press, 2001).
73. Pruitt, K.D., Tatusova, T., Brown, G.R. & Maglott, D.R. NCBI Reference Sequences (RefSeq): current status, new features and genome annotation policy. *Nucleic Acids Res.* **40**, D130–D135 (2012).
74. Xie, X., Rigor, P. & Baldi, P. MotifMap: a human genome-wide map of candidate regulatory motif sites. *Bioinformatics* **25**, 167–174 (2009).
75. Matys, V. *et al.* TRANSFAC: transcriptional regulation, from patterns to profiles. *Nucleic Acids Res.* **31**, 374–378 (2003).
76. Portales-Casamar, E. *et al.* JASPAR 2010: the greatly expanded open-access database of transcription factor binding profiles. *Nucleic Acids Res.* **38**, D105–D110 (2010).
77. Krzywinski, M. *et al.* Circos: an information aesthetic for comparative genomics. *Genome Res.* **19**, 1639–1645 (2009).